THE ASTROPHYSICAL JOURNAL, 407:564–578, 1993 April 20

OPTICAL EMISSION-LINE PROPERTIES OF M33 SUPERNOVA REMNANTS[1]

R. CHRIS SMITH
Cerro Tololo Inter-American Observatory, Casilla 603, La Serena 1353, Chile
ROBERT P. KIRSHNER
Harvard-Smithsonian Center for Astrophysics, 60 Garden Street, Cambridge, MA 02138
WILLIAM P. BLAIR
Center for Astrophysical Sciences, The Johns Hopkins University, Baltimore, MD 21218
KNOX S. LONG
Space Telescope Science Institute, 3700 San Martin Drive, Baltimore, MD 21218
AND
P. FRANK WINKLER
Middlebury College, Department of Physics, Middlebury, VT 05753
Received 1992 September 1; accepted 1992 October 6

ABSTRACT

We have obtained spectra of the 42 supernova remnants (SNRs) and remnant candidates identified in the recent survey of the inner portion of M33. Relative fluxes for the important diagnostic emission lines in the red portion of the optical spectrum (6200–7500 Å) are reported. We have confirmed that all the candidate SNRs have [S II]/Hα ratios ≥ 0.4, the canonical dividing line between SNR emission and emission from the photoionized gas in H II regions and planetary nebulae. Significant [O I] emission, another distinguishing characteristic of shocked gas, is also seen in the majority of the remnants. We find little evidence of emission-line variation with SNR diameter, unlike that reported in previous SNR samples. Using published grids of shock models, we derive abundances and abundance gradients in the interstellar gas in M33. While the oxygen abundances and gradient derived agree (to within the rather large errors) with those derived from H II region studies, the nitrogen abundances and gradient show the same offset as previously noted in studies of other galaxies.

Subject headings: galaxies: abundances — galaxies: individual (M33) — H II regions — nebulae: supernova remnants

1. INTRODUCTION

Supernova remnants (SNRs) play an important role in our understanding of supernovae (SNs), the interstellar medium (ISM), and their interaction. The emission from young SNRs can reveal details of stellar and SN nucleosynthesis (Chevalier & Kirshner 1979; Kirshner & Winkler 1985; Blair et al. 1989), and the interaction of the SNR shock with circumstellar material can probe the mass loss history of the progenitor star (Bandiera 1987). With samples of SNRs, we can probe SNR evolution and derive estimates of SN rates and SN energies, as well as estimate the densities and density variations in the ISM (Dopita 1979; Fusco-Femiano & Preite-Martinez 1984).

Samples of SNRs can also be used to study ISM abundances and abundance gradients in our Galaxy (Binette et al. 1982; Fesen, Blair, & Kirshner 1985) and other galaxies (Blair, Kirshner, & Chevalier 1982; Dopita et al. 1984; Blair & Kirshner 1985). The optical emission from evolved remnants is due to shocks traveling into the ambient interstellar gas and thus probes ISM material, not the original SN ejecta. By comparing spectral observations of SNRs with shock models, such as those of Dopita et al. (1984), Raymond (1979), and Shull & McKee (1979), we can estimate the abundances of the interstellar material into which the SNRs are expanding. These studies provide an important check on abundances and gradients derived from observations of H II regions (e.g., Zaritsky, Elston, & Hill 1989, 1990 and references therein).

Such studies, however, require large samples of SNRs, especially to establish gradients and reduce errors due to local fluctuations in ISM conditions. While the galactic sample has grown to ~170 SNRs through diligent sifting of radio survey data (Green 1991 and references therein), most of this sample is observable only at radio wavelengths. Optical study of these SNRs is hampered by interstellar absorption, which limits the observable number to less than one-third of the total sample. In addition, distances to galactic SNRs are difficult to determine, and estimates can vary by an order of magnitude (Green 1984). These uncertainties in distances translate into uncertainties in diameters, hindering evolutionary analysis of the sample, and uncertainties in location within the Galaxy which interfere with abundance gradient analyses. These problems are significantly less severe in extragalactic samples, in which absorption problems can be minimized by studying face-on systems and the determination of both diameters and the locations of SNRs is greatly simplified.

Mathewson & Healy (1964) identified the first extragalactic SNR candidates in a radio survey of the LMC. The three candidates were confirmed by Westerlund & Mathewson (1966) using a combination of radio and optical techniques. The Magellanic Cloud SNR sample has since grown to 32 confirmed remnants in the LMC and 11 in the SMC using a combination of radio, X-ray, and optical identification methods (Mathewson et al. 1983, 1984, 1985, and references

[1] Based partly on observations obtained at the Multiple Mirror Telescope Observatory, a joint facility of the Smithsonian Astrophysical Observatory and the University of Arizona.

therein). For more distant galaxies, however, radio and X-ray surveys have failed to identify significant numbers of new SNRs due to sensitivity and resolution limitations (Goss et al. 1980; Long et al. 1981; Cowan & Branch 1985), so most surveys have relied on optical identification techniques. These optical studies have taken advantage of the strong [S II] emission relative to Hα present in the cooling regions of shocks to distinguish SNRs from other nebulosities. Galactic SNRs typically have [S II]/Hα ratios $\gtrsim 0.4$, while photoionized nebulae usually exhibit ratios of less than 0.1.

Optical surveys have been undertaken covering several local group galaxies beyond the Magellanic Clouds using photographic observations through narrow-band Hα and [S II] filters to identify candidate nebulosities. D'Odorico, Benvenuti, & Sabbadin (1978) pioneered such searches, identifying three SNRs in the southern arm of M33. In successive surveys (Sabbadin 1978; Sabbadin & Bianchini 1979; Sabbadin 1979; D'Odorico, Dopita, & Benvenuti 1980; Blair, Kirshner, & Chevalier 1981), 21 candidates were identified in M31, 37 in M33, and several others in six other Local Group galaxies. For the brightest of these candidates, radio and X-ray observations have confirmed the SNR identifications (Goss et al. 1980; D'Odorico, Goss, & Dopita 1982; Markert & Rallis 1983; Trinchieri, Fabbiano, & Peres 1988). Most of the candidates, however, have fallen below the sensitivity limits of the radio and X-ray observations and thus could be confirmed only by optical spectroscopy (Dopita, D'Odorico, & Benvenuti 1980, hereafter DDB; Blair et al. 1981, 1982; Blair & Kirshner 1985, hereafter BK) showing that the spectra of the SNR candidates resembled spectra of known galactic remnants.

Improvements in detectors and techniques in the past decade have made optical surveys for extragalactic SNRs more feasible. The sensitivity and linearity of CCDs allow both image and spectral observations to extend down to much fainter surface brightnesses and probe more confused regions such as H II regions and the central regions of galaxies. We have therefore begun a systematic survey of nearby galaxies in search of SNRs to provide samples which may be used to investigate SNR evolution as well as probe SN, SNR, and ISM interactions.

M33 is an obvious galaxy in which to begin such a search. At approximately 720 kpc[2] (de Vaucouleurs 1978), 1″ equals ~3.5 pc so that all but the smallest remnants are spatially resolved. Also, its low inclination ($i = 57°$; Searle 1971; Kent 1987) reduces absorption problems. These advantages have contributed to the identification of 37 candidates from photographic surveys of M33 mentioned above. Of these, 13 have been confirmed with optical spectroscopy (Danziger et al. 1979; DDB; BK). Radio searches to identify new SNRs in M33 have been unsuccessful in the past, but eight optically identified remnants have been detected at radio wavelengths (Goss et al. 1980; D'Odorico et al. 1982; Goss & Viallefond 1985; Viallefond et al. 1986; Reynolds & Fix 1987), and recent observations with the VLA and Westerbork arrays show promising results (Duric 1988; Gordon 1991). X-ray observations have similarly failed to identify significant numbers of SNRs, with only two confirmed SNRs identified from the 17 sources detected (Long et al. 1981, Markert & Rallis 1983; Trinchieri et al. 1988). We therefore chose to perform an optical survey of M33 using CCD imaging with interference filters to identify SNRs.

In our previous paper (Long et al. 1990, hereafter Paper I), we presented an atlas of SNRs and SNR candidates selected from our CCD imaging survey of the central 15′ of M33. We identified 42 emission nebulae which showed strong [S II] emission relative to Hα ([S II]/Hα ≥ 0.4), of which 12 are previously identified SNRs and candidates and 30 are new SNR candidates. While our CCD observations produced [S II]/Hα ratios far more accurate than those from photographic surveys, spectral confirmation is still necessary due to contamination of Hα flux measurements by [N II] emission and difficulties in background determination.

In this paper, we report on the spectroscopic confirmation of all of the SNRs and SNR candidates identified in Paper I and discuss the emission-line properties of this uniform sample. We provide a review of the imaging survey in § 2 and summarize the spectral observations in § 3. In § 4, we discuss the observed range of [S II]/Hα and its implications for the identification of SNRs. Variations in emission-line ratios with SNR evolution and abundances are examined in § 5, along with the abundances and the abundance gradient in the disk of M33. A summary of our results is given in § 6, along with a discussion of future investigations.

2. REVIEW OF THE IMAGING SURVEY

To identify SNRs optically, one looks for the spectral signature of shocked gas cooling—strong hydrogen recombination lines combined with strong forbidden emission lines from oxygen, nitrogen, and sulfur. SNRs share this general description with at least two other types of gaseous nebulae, planetary nebulae (PNs) and the ubiquitous H II regions, even though the processes leading to the emission are quite different. However, the photoionizing radiation in H II regions and PNs keeps coolant elements in relatively high ionization states, such as O^{++}, S^{++}, and N^{++}. In SNRs, while shocks heat the gas to high temperatures and atoms are collisionally ionized to these states, the cooling time is short in the dense clouds which account for most optical filaments, and thus emission from low ionization states is also strong relative to the H recombination lines. We can therefore differentiate SNRs from photoionized nebulae by comparing optical emission from [O I], [O II], [S II], and other neutral or singly ionized species.

The ratio of [S II] λλ6717, 6731 to Hα has become the standard discriminator used in optical SNR surveys because of the strength of these lines and the comparative ease with which they may be observed. Mathewson & Clarke (1972, 1973) pioneered the use of [S II] to Hα comparison in their identification of SNRs in the LMC and SMC. The basis for the separation between SNRs and photoionized nebulae was largely empirical. Photoionized nebulae usually exhibit [S II]/Hα ratios of about 0.1, while known Galactic SNR (confirmed with radio and/or X-ray observations) show ratios typically >0.4. Theoretical shock models (Dopita 1977; Raymond 1979; Shull & McKee 1979) have supported the separation, generally predicting [S II]/Hα ratios of 0.5 to 1.0. Based on both the Galactic and LMC SNR samples, D'Odorico (1978) argued that a division at [S II]/Hα = 0.4 provides clear distinction of SNRs from photoionized regions despite the differing abundances between the Galaxy and the LMC. Subsequent use of this discriminant in photographic surveys has proven successful in several local group galaxies (D'Odorico et al. 1980; Blair et al. 1981). Spectroscopic observations of the identified nebulae have usually

[2] Although recent distance determinations (see van den Bergh 1991) indicate that the actual distance may be closer to 800 kpc, we continue to use 720 kpc for consistency with Long et al. 1990 (Paper I).

shown additional evidence of shock emission, such as strong [O I] emission or high [O III] electron temperatures.

The advantages of CCDs over previously used photographic techniques present the opportunity to use more quantitative methods to select nebulosities with [S II]/Hα ≥ 0.4. Using the KPNO 4 m telescope with the prime focus camera and the 800 × 800 pixel TI-2 CCD, we obtained images of 18 fields covering the central 250 arcmin^2 of M33 in the light of Hα, [S II], [O III], and a continuum band centered at 6100 Å. The images were taken during two observing runs, 1986 September and 1987 November, with slightly different filter sets (see Table 1 in Paper I). In both sets, the Hα filter also allowed some [N II] λ6548 and λ6584 emission to pass through the filter as well.

Preliminary SNR candidates were identified by blinking the images and selecting nebulosities with strong [S II] relative to Hα (actually Hα + some [N II]). The continuum image was then checked to confirm that the objects had no continuum since such emission contributes roughly equally to the [S II] and Hα bandpasses and produces spuriously high [S II]/Hα ratios. While this is the same technique used in photographic studies, the large dynamic range of the CCD data and the ability to vary the display of the image greatly enhanced our sensitivity to diffuse, low surface brightness nebulosities. Approximately 50 preliminary candidates were identified in this manner.

The [S II]/Hα ratio for each of these initial candidates was then determined from the images. The ratio was measured in continuum-subtracted and background-subtracted images. Only the brightest portion of each object was used in order to minimize problems due to background subtraction. Corrections to the measured ratios were necessary to allow for the [N II] contamination (to first order) as well as the different transmission efficiencies of the two filter sets used. Of the ~50 initial candidates, 42 were shown to have [S II]/Hα ≥ 0.4. Since the uncertainty of the ratio determination from images was estimated to be roughly ±0.1, the three objects with ratios of 0.4 were considered marginal candidates while the rest, with [S II]/Hα ≥ 0.5, were described as excellent candidates. Among the 42 objects identified were 10 previously confirmed SNRs (DDB; BK) and two unconfirmed candidates (Sabbadin 1979). Thus, with 30 new SNR candidates, our imaging CCD survey more than tripled the number of identified remnants and candidates in the inner portion of M33 and pushed the sensitivity limit down to $\sim 1 \times 10^{-16}$ ergs cm^{-2} s^{-1} arcsec^{-2}.

While the [S II]/Hα ratios derived from our CCD imagery are far more accurate than those derived photographically, uncertainties remain due to difficult background subtraction and filter correction factors. The line emission from nebulae is contaminated by individual stars as well as diffuse background starlight and diffuse H II emission in M33. Uncertainties in estimates of these backgrounds translate directly into uncertainties in our derived ratios. Several candidates are located near or even in H II regions, making accurate background subtraction significantly more difficult.

These difficulties are compounded by uncertainties in filter transmission in the f/2.7 beam of the KPNO 4 m telescope, which shifts the passband of the filters to shorter wavelengths by approximately 15 Å and changes the passband shape (Jacoby 1987). These effects complicated efforts to correct for contamination of Hα fluxes by [N II] emission and to correct for the differences in filter sets. A comparison of the [S II]/Hα ratios derived from our images with those measured spectroscopically in nine previously identified SNRs showed that our background and filter transmission corrections successfully put the 1986 and 1987 data sets on a common scale to within the errors, and that only a small (<10%) systematic bias existed between the image and spectral ratios. While this agreement is promising, spectra are nevertheless required to verify the [S II]/Hα ratios as well as to provide additional evidence to differentiate the SNRs from photoionized nebulae.

3. SPECTRAL OBSERVATIONS

3.1. *Observations and Reductions*

The spectroscopic observations of the M33 SNRs and candidates were made with the Multiple Mirror Telescope (MMT) and the Red Channel long-slit CCD spectrograph (Schmidt, Weymann, & Foltz 1989) over a period of 2 years, from 1988 October to 1990 November. A red-blazed 600 lines mm^{-1} grating provided a resolution of approximately 7 Å with a spectral coverage of about 1300 Å, usually from about 6200 to 7500 Å. The resolution and spectral coverage were chosen to allow separation of the [N II] lines from Hα for accurate measurement of the [S II]/Hα ratio and other ratios relative to Hα, as well as to resolve [S II] lines for determination of the density sensitive [S II] λ6717/6731 ratio. The TI 800 × 800 pixel CCD was binned by 2 pixels in the spatial direction yielding 0.″6 pixels. Slit positions and position angles were chosen to include the brightest portions of the objects while minimizing H II region contamination. In many cases, we positioned the slit to include nearby emission regions (usually faint H II regions). For each observation, the slit was positioned by offsetting from a nearby star since most of the SNR candidates were invisible on the acquisition television. Table 1 contains a summary of the spectroscopic observations, including slit widths used and the resulting resolutions.

All data reduction was performed using IRAF.[3] After subtracting overscan regions and bias frames, cosmic rays were removed and the images were divided by normalized dome flats to correct for pixel-to-pixel variations in sensitivity. All images showed significant instrumental curvature in the spatial direction, so the data were rectified using the comparison lines to map the distortion. Distortions in the spectral direction were generally less than 2 pixels and thus were not corrected since they were small in comparison to the sizes of our objects. A general background was removed from the two-dimensional images by fitting low-order polynomials in the spatial direction, constrained by the portions of the slit containing only sky. This process removed some diffuse background H II emission as well as diffuse sky emission and sky lines.

The images were corrected for atmospheric extinction and then were flux-calibrated using observed calibration standards from IRAF's IRSCAL data base. Comparison of flux standards often showed significant variation throughout the nights due to nonphotometric conditions, so our absolute fluxes are only accurate to within about a factor of 2. However, in all cases the sensitivity functions (the correction for wavelength-dependent sensitivity of the CCD) for different standards agreed to within 1%, indicating that our sensitivity correction, which are important for deriving accurate line *ratios*, are good at approximately this level.

[3] IRAF is distributed by the National Optical Astronomy Observatories, which is operated by the Association of Universities for Research in Astronomy, Inc. (AURA) under cooperative agreement with the National Science Foundation.

TABLE 1

OBSERVATION LOG

Night	Slit Width (arcsec)	[O I] Resolution (Å)	Hα Resolution (Å)	[S II] Resolution (Å)	Resolution at λ7200 Å (Å)
1988 Oct 02	1.5	7.1	5.4	5.4	5.6
1988 Oct 03	1.5	7.3	5.4	5.4	5.6
1988 Dec 13	1.5	7.8	5.4	5.4	5.4
1988 Dec 14	1.5	8.7	5.9	5.4	5.9
1988 Dec 15	1.5	9.4	6.1	5.4	5.9
1988 Dec 16	1.5	8.9	5.9	5.4	5.6
1989 Sep 04	2.0	7.1	7.1	7.5	7.1
1989 Sep 07	2.0	7.3	7.1	7.3	7.1
1989 Nov 05	2.0	8.5	7.5	7.3	7.1
1989 Nov 06	2.0	8.0	7.3	7.3	6.8
1989 Nov 07	2.0	8.0	7.3	7.3	7.1
1990 Nov 11	2.0	7.1	7.5	8.2	...
1990 Nov 13	2.0	7.1	7.3	7.1	...

NOTE.—Resolutions based on HeNeAr comparison spectra.

One-dimensional spectra were then extracted from the two-dimensional flux-calibrated images. Since the images had been distortion-corrected and background-subtracted, the extraction generally involved simply summing over the desired area along the slit. However, in cases where the candidate was situated in significant localized H II region emission, an additional background was subtracted as determined from the adjacent H II emission. Figure 1 shows representative spectra from our sample, from one of our best spectra (a bright, previously known SNR) to average and worse-than-average spectra. A spectrum of an H II region in M33 is also shown for comparison.

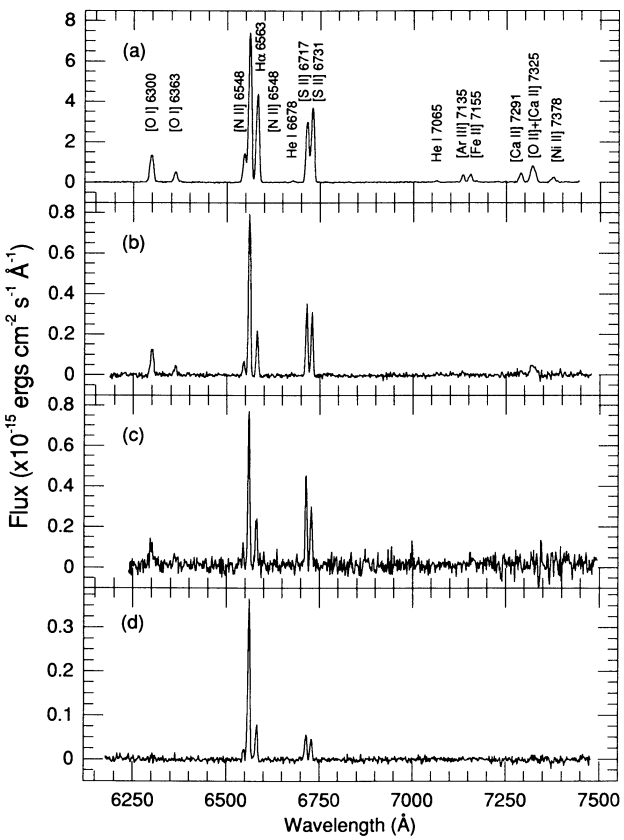

FIG. 1.—Spectra from our sample of SNRs (and H II regions) in M33: (*a*) SNR 013042+30182, a previously known remnant and one of the brightest in the sample; (*b*) SNR 013022+30224, with a spectrum of typical quality from our sample; (*c*) SNR 013113+30157, one of the less well observed remnants; and (*d*) for comparison, an H II region in M33.

3.2. *Flux Measurement*

Line strengths were measured in the one-dimensional spectra by two methods. The strong, somewhat blended lines of Hα+[N II] λλ6548, 6584 and [S II] λλ6717, 6731 were fitted with Gaussians. The weak lines, most importantly [O I] λλ6300, 6363, were measured by simply summing the flux at the nominal line position.

The Gaussian fits to determine the Hα, [N II], and [S II] fluxes were made using a general χ^2 minimization routine. For the Hα+[N II] blend, three Gaussians were fitted with one center, one width (σ), three fluxes, and a zero offset (constant continuum). The Hα line center was fitted (nominally at λ6562.8), with constant offsets of $\Delta\lambda = -14.7$ Å for [N II] λ6548.1 and $\Delta\lambda = +20.6$ Å for [N II] λ6583.4. The wavelengths quoted here and elsewhere in this paper are corrected for the 4 Å blueshift imposed by the velocity of M33 (-181 km s^{-1}; de Jaeger & Davies 1971; Deul & van der Hulst 1987). The zero offset was included to compensate for the slight nonzero "continuum" level present in some of the spectra due to incomplete (or overestimated) background subtraction. The [S II] blend was fitted similarly but with only two fluxes, or a total of five fit parameters. The red component (line center nominally λ6730.8) was fitted with a fixed line separation of $\Delta\lambda = 14.4$ Å. The total fluxes from all of these fits were found to be within 1% of the total observed fluxes (summed over the blended lines) in all but the lowest signal-to-noise ratio spectra.

In most cases, the [O I] λλ6300, 6363 lines did not lend themselves to Gaussian fitting, both because of their faintness and because of the effects of sky subtraction, which often did not leave Gaussian profiles for the remaining source [O I] flux. The lines were well separated in our spectra, so blending was not a problem. In lieu of fitting, we measured the flux by summing the data into 25 Å wide bins centered on the 4 Å blueshifted line centers. The width of the bins was set by

the 3 σ width of the lines in 013042+30182, the remnant with the broadest lines in our survey, as well as to allow for shifts in the lines. Sky bins were also extracted, and the mean of the sky bins was subtracted from the line bins to account for any background subtraction errors (analogous to the zero offset used above). The RMS of the sky bins was used as a "sky sigma," and [O I] λ6300 lines with a net flux greater than 3 times this sky sigma were considered detections. This method was also used to measure the usually extremely weak lines of He I λ6678 and λ7065, [Ar III] λ7135, [Fe III] λ7172, [Ca II] λ7291, [Ni II] λ7378, and the [O II] + [Ca II] blend at λ7325.

The results of these flux measurements, both Gaussian fits and binning, are summarized in Table 2. All fluxes are scaled to a Hα flux of 300 for comparison with other work. Note that we have made no corrections for extinction in our Galaxy or in M33. However, within our limited wavelength coverage, any correction would be $\lesssim$3% based on previous data sets (DDB; BK). Including this uncertainty, the relative fluxes given in Table 2A are good to better than 15% except where indicated. The fluxes of the weak lines given in Table 2B have uncertainties of a factor of 2 or larger and are meant mainly to indicate detections of the lines. As mentioned previously, the absolute Hα fluxes are only good to within a factor of 2 due to variations in observing conditions. In Table 3, we present several diagnostic line ratios derived from our measured fluxes.

3.3. *Comparison with Previous Measurements*

Since spectral confirmation of the [S II]/Hα ratios derived from our narrow-band images was a major motivation for this study, we first compare the results of the two methods to determine how good the image ratios actually are. While the image ratios required a correction for [N II] emission in the Hα images, our spectral resolution cleanly separates the Hα from the [N II] lines, allowing for far more accurate [S II]/Hα measurement. As shown in Figure 2, the [S II]/Hα ratios derived from the images are mostly consistent with the spectral values to within the scatter of the estimates. The mean difference is only 0.05 for [S II]/Hα $\lesssim$ 1.0. For [S II]/Hα ratios of about 1.0 and larger, most image ratios are systematically and significantly lower than the spectral ratios. These objects also have among the strongest [N II]/Hα ratios. Stronger [N II] emission produces a larger contamination of the flux measured in the Hα image and hence a larger estimate of Hα emission. Since the [N II]/Hα and [S II]/Hα ratios are correlated, as shown in Figure 3, the accuracy of the image [S II]/Hα ratios decreases with increasing [S II]/Hα ratios. For the SNRs and candidates

TABLE 2A

OBSERVED FLUXES RELATIVE TO Hα = 300 FOR STRONG EMISSION LINES

SNR	[O I] 6300	[O I] 6363	[N II] 6548	Hα	[N II] 6584	[S II] 6717	[S II] 6731	Hα flux[a]
013004+30226	20.7	6.2	10.8	300.0	52.0	107.1	74.6	1.12E-14
013004+30228	28.4:	15.0:	23.6	300.0	63.8	97.6	66.0	4.80E-15
013007+30252	62.4:	24.7:	13.6	300.0	49.3	143.9	97.9	9.57E-15
013008+30241	52.4	21.6	20.3	300.0	65.2	121.2	106.3	1.15E-14
013015+30245	46.9:	15.5:	24.0	300.0	67.0	94.0	54.4	2.03E-14
013021+30241	< 20.2	< 6.7	25.9	300.0	89.5	114.2	83.0	3.34E-15
013021+30270	74.9	31.5	31.3	300.0	82.1	165.5	116.0	2.91E-15
013022+30190	15.7:	5.0:	23.5	300.0	72.8	89.1	58.1	1.71E-14
013022+30244	62.6	20.4	25.9	300.0	81.1	121.7	107.8	5.86E-15
013040+30269	112.1	36.3	44.2	300.0	131.3	178.8	161.5	1.66E-14
013042+30182	67.0	24.1	58.5	300.0	179.3	125.9	154.1	7.29E-14
013042+30269	< 46.5	< 19.1	11.9	300.0	64.8	119.8	74.3	2.77E-15
013047+30211	47.5	13.2	46.9	300.0	143.9	155.7	141.2	7.07E-14
013048+30175	92.7	34.7	42.3	300.0	124.8	224.4	156.9	3.59E-15
013049+30248	76.4	33.6:	40.8	300.0	145.7	195.7	136.5	1.76E-15
013049+30270	27.7:	13.3:	26.6	300.0	92.6	114.9	81.8	6.63E-15
013052+30272	14.4:	7.1:	32.5	300.0	100.0	108.3	75.0	1.94E-14
013055+30208	< 14.4	< 9.7	28.0	300.0	82.3	95.0	67.7	1.07E-14
013059+30177	36.4	13.8	29.1	300.0	92.0	130.9	91.5	8.41E-15
013101+30201	37.4	14.1:	37.6	300.0	120.0	142.3	105.2	4.05E-15
013102+30285	19.2:	2.2:	32.7	300.0	104.4	111.9	77.5	1.01E-14
013105+30185	45.3	13.8	28.8	300.0	89.3	148.3	105.2	1.05E-14
013106+30178	49.6	18.7	35.8	300.0	108.2	132.3	118.2	1.45E-14
013108+30196	120.0	39.3	37.3	300.0	124.1	260.8	186.4	3.75E-15
013109+30168	< 15.2	< 5.1	23.2	300.0	66.5	71.1	49.1	1.19E-14
013109+30225	100.9	34.6	58.0	300.0	179.6	235.4	177.8	5.04E-15
013110+30182	20.7:	12.8:	32.7	300.0	100.6	129.4	89.7	1.57E-14
013110+30210	119.4	46.1	62.4	300.0	198.7	235.1	193.2	2.58E-15
013111+30270	52.6:	14.6:	60.8	300.0	188.7	230.3	165.4	3.59E-15
013113+30157	72.9:	29.8:	30.0	300.0	98.9	171.6	115.5	4.76E-15
013114+30294	< 28.1	< 17.5	33.3	300.0	148.7	178.9	130.7	2.40E-15
013118+30210	46.2:	11.6:	28.3	300.0	85.2	122.9	90.8	1.20E-14
013121+30271	119.0	40.1	41.8	300.0	134.0	200.6	174.4	2.01E-14
013124+30198	< 30.4	< 11.4	25.4	300.0	82.6	92.1	47.3	2.82E-15
013124+30281	21.3:	14.9:	35.4	300.0	116.7	145.9	116.5	2.35E-15
013125+30192	13.1	6.9	19.2	300.0	57.6	81.6	57.5	1.48E-14
013125+30244	89.2	15.5:	41.1	300.0	115.9	189.8	126.6	3.12E-15
013125+30266	59.6:	19.2:	49.8	300.0	132.0	184.8	137.7	1.80E-15
013126+30176	31.9:	21.3:	35.9	300.0	97.3	134.0	89.5	1.30E-15
013128+30260	55.1	19.7:	43.7	300.0	130.6	184.7	126.0	5.63E-15
013130+30184	22.1:	6.5:	23.8	300.0	64.5	108.4	76.5	1.12E-14
013131+30186	37.1	12.9	25.7	300.0	74.6	130.2	91.2	1.88E-14

NOTE.—Colon indicates larger uncertainty due to sky subtraction difficulties.

[a] Hα flux in ergs s^{-1} cm^{-2}.

TABLE 2B

OBSERVED FLUXES RELATIVE TO Hα = 300 FOR WEAK EMISSION LINES[a]

SNR	He I 6678	He I 7065	[Ar III] 7135	[Fe II] 7155	[Ca II] 7291	[O II]+[Ca II] 7325	[Ni II] 7378
013007+30252	...	...	...	...	...	0.10	...
013008+30241	...	...	...	0.03	0.04	0.12	...
013022+30244	...	...	0.03	...	0.06	0.15	...
013040+30269	...	0.02	0.02	0.04	0.08	0.14	0.03
013042+30182	0.01	0.01	0.05	0.07	0.07	0.18	0.04
013047+30211	0.01	0.02	0.03	0.03	0.05	0.11	0.03
013049+30248	...	...	...	...	...	0.20	...
013055+30208	0.01	...	...	...	...	...	...
013102+30285	0.03	...	...	...	...	...	...
013106+30178	...	...	...	...	...	0.07	...
013108+30196	...	...	...	...	0.08	0.14	...
013109+30225	...	...	...	...	0.07	0.13	...
013110+30210	...	...	...	...	0.11	0.14	...
013114+30294	...	...	...	...	...	0.17	...
013121+30271	...	...	...	...	0.04	0.14	...
013126+30176	...	...	...	...	...	0.19	...
013128+30260	...	...	...	...	0.15	0.22	...
013130+30184	...	...	0.05	...	...	...	...
013131+30186	...	...	0.03	...	...	0.03	...

[a] Relative fluxes are good to only a factor of 2 due to weakness of these lines. Only lines with signal >3 times sky RMS listed.

with [S II]/Hα $\lesssim$ 1.0, the image ratios are good to about $\pm$0.1. It is important to note that although the accuracy of the image ratios decreases for [S II]/Hα $\gtrsim$ 1.0, this does not impact the ability to identify SNRs, since such objects are well above the threshold of 0.4. The techniques used to identify these candidates do therefore provide an accurate method of determining nebular intensity ratios to distinguish SNRs from photoionization nebulae, in spite of the difficulties of low surface brightness and confusion. In fact, there is no indication that the ratios measured from the images are significantly less accurate at low surface brightness than at high surface brightness.

Comparison of our data with previous spectra (DDB; BK) shows considerable differences for many of the SNRs in common between the three data sets. Figure 4 shows the scatter in four of the ratios: [O I]/Hα, [N II]/Hα, [S II]/Hα, and [S II] λ6717/6731. While the scatter is fairly large, there do not seem to be any *systematic* differences between the data sets over the wavelength range of our spectra. There is a slight tendency toward higher ratios in the DDB data, as noted by BK, but the scatter is much larger than the mean difference. In general, the BK data tend to have less scatter, but differences as large as 20%–50% are still present. Some of these differences may be attributable to the lower resolution and/or lower signal-to-noise ratios of previous spectra. It is likely, however, that the differences can be at least partly due to the inclusion or exclusion of different filaments in the identified SNRs. Since, in many cases, the SNRs or candidates are associated with faint H II emission, the inclusion of this faint nebulosity may significantly alter the derived ratios (especially those involving Hα). With our long-slit CCD observations, we have been careful to extract only emission identified with the SNR and have attempted to subtract background H II emission where the SNR is apparently embedded within it.

4. SNRS OR H II REGIONS

Of the 42 objects we cataloged in Paper 1, 30 were new SNR candidates and two were previously identified, but uncon-

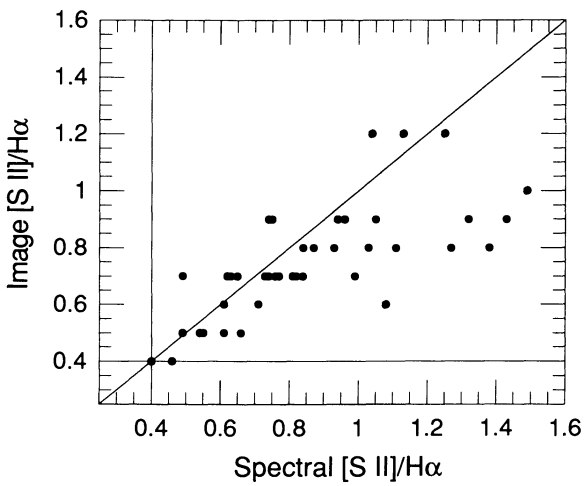

FIG. 2.—A comparison of the [S II]/Hα ratios measured from the imaging survey vs. the more accurate spectral determinations. The image ratios prove to be good measurements except at high [S II]/Hα, where the correction for contamination of the Hα by [N II] breaks down.

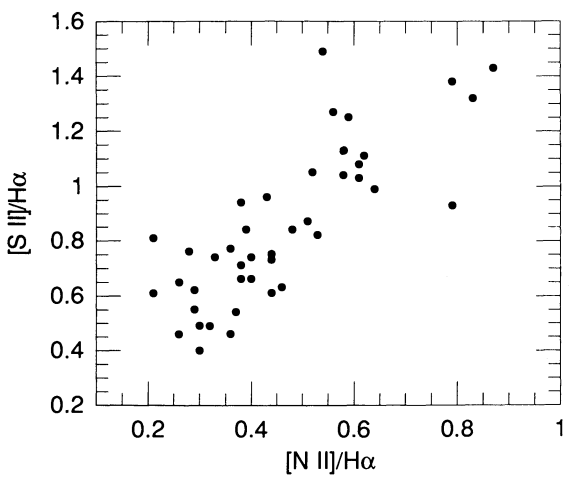

FIG. 3.—The observed correlation of [N II]/Hα with [S II]/Hα. As [S II]/Hα increases, the [N II] contamination in the Hα filter increases, leading to low [S II]/Hα estimates from comparison of the Hα and [S II] images.

TABLE 3

INTENSITY RATIOS FOR M33 SNRs

SNR	Diam (pc)	[O I]/Hα	[N II]/Hα	[S II]/Hα	6731/Hα	6717/6731
013004+30226	44.00	0.09	0.21	0.61	0.25	1.43
013004+30228	48.00	0.14:	0.29	0.55	0.22	1.48
013007+30252	100.00	0.29:	0.21	0.81	0.33	1.47
013008+30241	12.60	0.25	0.28	0.76	0.35	1.14
013015+30245	24.00	0.21:	0.30	0.49	0.18	1.50[a]
013021+30241	55.00	< 0.09	0.38	0.66	0.28	1.38
013021+30270	18.50	0.35	0.38	0.94	0.39	1.43
013022+30190	82.00	0.07:	0.32	0.49	0.19	1.50[a]
013022+30244	11.50	0.28	0.36	0.77	0.36	1.13
013040+30269	10.50	0.49	0.58	1.13	0.54	1.11
013042+30182	34.00	0.30	0.79	0.93	0.51	0.82
013042+30269	55.00	< 0.22	0.26	0.65	0.25	1.50[a]
013047+30211	29.00	0.20	0.64	0.99	0.47	1.10
013048+30175	30.00	0.42	0.56	1.27	0.52	1.43
013049+30248	39.00	0.37	0.62	1.11	0.46	1.43
013049+30270	20.00	0.14:	0.40	0.66	0.27	1.40
013052+30272	84.00	0.07:	0.44	0.61	0.25	1.44
013055+30208	21.00	< 0.08	0.37	0.54	0.23	1.40
013059+30177	28.00	0.17	0.40	0.74	0.30	1.43
013101+30201	38.00	0.17	0.53	0.82	0.35	1.35
013102+30285	50.00	0.07:	0.46	0.63	0.26	1.44
013105+30185	36.00	0.20	0.39	0.84	0.35	1.41
013106+30178	16.80	0.23	0.48	0.84	0.39	1.12
013108+30196	27.00	0.53	0.54	1.49	0.62	1.40
013109+30168	18.00	< 0.07	0.30	0.40	0.16	1.45
013109+30225	15.00	0.45	0.79	1.38	0.59	1.32
013110+30182	18.00	0.11:	0.44	0.73	0.30	1.44
013110+30210	6.30	0.55	0.87	1.43	0.64	1.22
013111+30270	29.00	0.22:	0.83	1.32	0.55	1.39
013113+30157	46.00	0.34:	0.43	0.96	0.39	1.49
013114+30294	36.00	< 0.15	0.61	1.03	0.44	1.37
013118+30210	89.00	0.19:	0.38	0.71	0.30	1.35
013121+30271	19.00	0.53	0.59	1.25	0.58	1.15
013124+30198	57.00	< 0.14	0.36	0.46	0.16	1.50[a]
013124+30281	26.00	0.12:	0.51	0.87	0.39	1.25
013125+30192	29.00	0.07	0.26	0.46	0.19	1.42
013125+30244	30.00	0.35	0.52	1.05	0.42	1.50
013125+30266	39.00	0.26:	0.61	1.08	0.46	1.34
013126+30176	26.00	0.18:	0.44	0.75	0.30	1.50
013128+30260	43.00	0.25	0.58	1.04	0.42	1.47
013130+30184	10.00	0.10:	0.29	0.62	0.26	1.42
013131+30186	21.00	0.17	0.33	0.74	0.30	1.43

NOTE.—Colon indicates larger uncertanty due to sky subtraction difficulties.

[a] Aphysical line ratio (> 1.5); set to high-ratio limit (low-density limit).

firmed, candidates. Above, we have confirmed spectroscopically that all of these candidates satisfy the canonical criterion for identification as SNRs, [S II]/Hα ≥ 0.4 (Table 3). However, as shown in Figure 2, several of the remnants show [S II]/Hα ratios near the selection cutoff of [S II]/Hα = 0.4. Is this a sign of contamination by nebulae other than SNRs in our sample, or are such ratios consistent with the sample of known SNRs?

The specific value of [S II]/Hα used to discriminate SNRs from photoionized nebulae has been set empirically by comparing observations of known SNRs (objects with radio and/or X-ray properties characteristic of SNRs) and H II regions. Such comparisons (e.g., D'Odorico 1978) have pointed to the gap centered [S II]/Hα = 0.4–0.5 between the two types of objects, with SNRs typically well above and H II regions well below this ratio. Shock models (Raymond 1979; Shull & McKee 1979; Dopita et al. 1984) have corroborated this separation, showing that most radiative shocks exhibit high [S II]/Hα. There are, however, several Galactic and LMC remnants which fall below the nominal division, such as OA 184 (D'Odorico & Sabbadin 1977; Fesen et al. 1985, hereafter FBK) and Balmer-dominated SNRs. It is therefore not unexpected that our sample extends down to the lower bound we imposed. Indeed, we have probably excluded a few remnants in our efforts to exclude photoionized gas (discussion of the *completeness* of this sample is reserved for a later paper).

Typical H II regions, both Galactic (Hawley 1978) and extragalactic (McCall, Rybski, & Shields 1985), have [S II]/Hα ratios ~0.1. The largest ratios observed in either of these samples is ~0.3. In Figure 5, we show the [S II]/Hα ratios of the H II regions in M33 observed by DDB and Kwitter & Aller (1981) compared to the ratios of our SNR candidates. A significant gap remains between these bright H II regions and the SNRs in our sample.

Comparison of the strength of [O I] λλ6300, 6363 emission has been suggested as another technique to discriminate

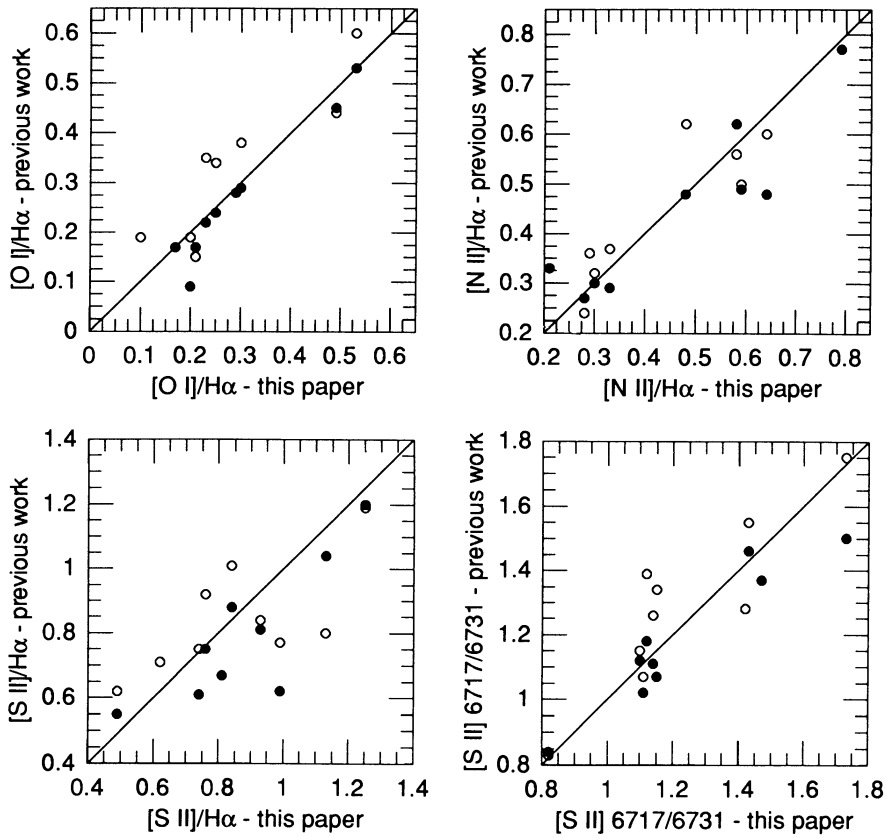

FIG. 4.—A comparison of our results with previous measurements. *Solid circles*: Blair & Kirshner (1985); *open circles*: Dopita, D'Odorico, & Benvenuti (1980). While the scatter is large for both samples, no systematic offsets are evident.

between SNRs and H II regions (and other photoionized nebulae), especially when combined with [O II] $\lambda\lambda$3726, 3729 observations (FBK). Although our spectral coverage does not include the [O II] lines, we have attempted to use the [O I] lines as a secondary discriminator to distinguish SNRs from other nebulae. In photoionized nebulae, the [O I] line is generally extremely weak, since most of the oxygen is in O^{++}, while in SNRs it is typically of order 10%–50% the strength of Hα.

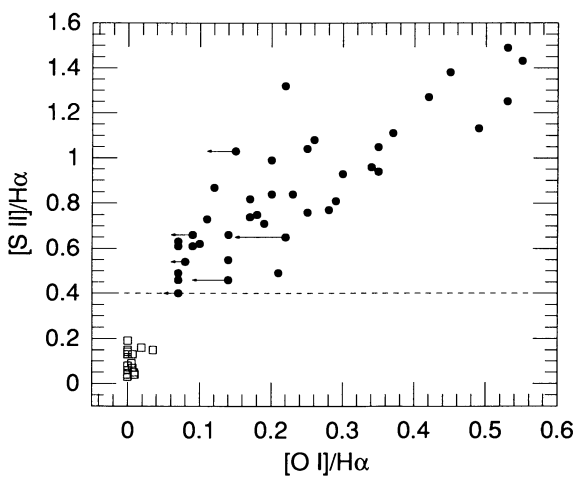

FIG. 5.—[S II]/Hα and [O I]/Hα ratios from our sample of SNR candidates (*filled circles*) compared to those from the H II regions (*open squares*) observed by Kwitter & Aller (1981) and DDB.

However, accurate measurement of the [O I] lines is hampered by the extremely strong night sky [O I] emission. While the 4 Å blueshift of the lines due to the velocity of M33 helps, accurate [O I] measurements were difficult. We nevertheless were able to obtain moderately accurate [O I] emission measurements for most of the candidates (see Table 2). Only six candidates showed little or no evidence (<3 times the sky RMS) of [O I] lines, and in these cases the upper limit is consistent with significant [O I] emission. The range of [O I]/Hα ratios measured for our candidates is similar to that observed in Galactic SNRs (see FBK Fig. 3) and separate from that of bright H II regions in M33 (Fig. 5).

It is apparent from Figure 5 that we have no problem spectrally differentiating SNRs from fairly bright, well-defined H II regions. However, these H II regions are among the brightest in M33 and are thus likely to be highly ionized. Faint, low-ionization H II regions may have higher [S II]/Hα ratios since less of the sulfur will be ionized up to S^{++}. To investigate the possible confusion, we extracted spectra of faint emission regions (FEMs) observed to be distinct from the SNRs in our long-slit spectra. The range of both [S II]/Hα and [O I]/Hα did tend to fill up the gap between the bright H II regions and the SNRs in Figure 5, although some of the larger ratios are undoubtably due to the large uncertainties in the ratios determined from the low signal-to-noise ratio spectra of these FEMs. In our images, most of the FEMs appear to be only marginally distinct from background fluctuations, with surface brightness of $\lesssim 1 \times 10^{-16}$ ergs cm^{-2} s^{-1} arcsec^{-2}. While these regions are distinct from our SNR sample based on morphological considerations (in blinking, we selected distinct struc-

tures as candidates) and surface brightnesses, the presence of these emission regions does pose a problem for SNR surveys probing to even lower surface brightnesses.

5. EMISSION-LINE VARIATIONS AND ISM ABUNDANCES

The [N II]/Hα and [S II]/Hα line ratios have been used extensively to estimate abundances in Galactic and extragalactic SNRs (BK, FBK, and references therein). These line ratios are thought to be accurate abundance tracers because, while they scale with abundance, they are relatively insensitive to shock conditions, especially shock velocity and gas density (Dopita et al. 1984, hereafter DBDB, and references therein). However, before using the ratios to estimate abundances, it is important to determine if there are other factors which may effect the relative line intensities, such as systematic effects due to SNR evolution.

5.1. *SNR Evolution or ISM Abundances?*

Daltabuit, D'Odorico, & Sabbadin (1976), D'Odorico & Sabbadin (1976), and Sabbadin (1977) claim that both Galactic and LMC SNRs show systematic variations in [N II]/Hα correlated with the density-sensitive [S II] λ6717/6731 ratio. They assert that both ratios are also correlated with remnant diameters, implying *evolutionary* trends in the ratios. While these relations have been dismissed as due to selection effects in the Galactic sample (FBK; Blair et al. 1982; Binette et al. 1982), the observed trend in the LMC has not been adequately explained.

Figure 6 shows the observed variation in [N II]/Hα versus λ6717/6731 in the remnants in our survey. Although both FBK and BK note a possible trend in the previous sample of M33 remnants, we see no evidence of any correlation in our more complete sample. If the general properties of SNRs in M33, the LMC, and our Galaxy are assumed to be similar, this result supports the claim of FBK that the observed trend in the galactic sample is due to selection effects.

While no relation is apparent in Figure 6, this does not rule out any evolutionary effects on intensity ratios. Figure 7 shows the abundance-sensitive and density-sensitive ratios observed in our present M33 sample as a function of remnant diameter. The uncertainties in the SNR diameters (which are large for a few of the remnants) should not affect this qualitative analysis. No significant linear correlation is evident. Certainly no linear *increase* with SNR diameter is present, as reported in the Galactic and LMC SNR samples by Daltabuit et al. (1976) and D'Odorico & Sabbadin (1976). All four diagrams do show a large scatter for smaller remnants than for large-diameter remnants and marginally smaller mean (*filled circles*) with increasing SNR diameter (the density-sensitive [S II] λ6717/6731 ratio has been plotted with density increasing upward). The reality of these trends is, however, dubious given the small numbers of remnants at larger diameters.

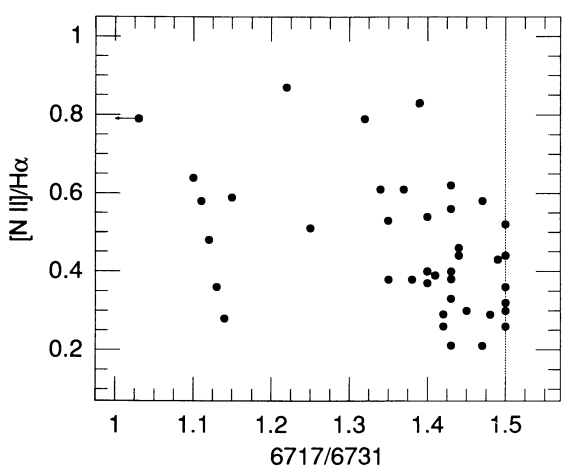

FIG. 6.—The observed [N II]/Hα ratios vs. [S II] λ6717/6731. The dotted line at λ6717/6731 = 1.5 indicates the low density limit of the ratio. Unlike samples of SNRs from the LMC and our Galaxy which show a linear trend, no correlation is apparent.

Moreover, such trends, evolutionary or not, should have little influence on abundance determinations other than to increase marginally the errors in our estimates. Almost 75% of the remnants have diameters less than 40 pc, a range in which there is little, if any, decrease in the mean of any of the abundance or density sensitive ratios. Also, as shown in Figure 8, there is no correlation between diameter and galactocentric distance R in the sample. The four largest diameter remnants span a range of galactocentric distances from 1.25 to 4.4 kpc. These positions (given in Table 4) are derived from the coordinates reported in Paper I together with an inclination of 57°, a position angle of 24° (Kent 1987), the center at $\alpha = 1^h31^m01^s.67$ and $\delta = 30°24'15''.0$ (de Vaucouleurs & Leach 1981), and a distance of 720 kpc (de Vaucouleurs 1978). Any diameter-dependent effects are therefore roughly orthogonal to variations with galactic radius. We performed the abundance analysis with a diameter-limited subset ($D < 40$ pc) to confirm that any diameter-dependent effects are minimal and found no differences in the results compared to those based on the whole sample.

5.2. *From Intensity Ratios to Abundances*

While SNs eject large amounts of processed material into the ISM, this enriched material is quickly overwhelmed by the interstellar matter swept up by the expanding blast wave. A simple calculation of the mass swept up,

$$M_{sw} = \tfrac{4}{3}\pi R^3 \rho \approx 0.12 n_0 R_{pc}^3 M_\odot ,$$

shows that all but the smallest remnant in our sample should have swept up much more interstellar material than was ejected for canonical values of ISM density and ejecta mass. Furthermore, theoretical models of SNRs indicate that a reverse shock driven back into the ejecta prevents it from keeping up with the blast wave (Gull 1973; McKee 1974; Chevalier 1975). The optical emission of evolved SNRs results from radiative shocks driven into the ambient interstellar material, and therefore is characterized by ISM abundances rather than the abundances of ejecta from SNs. Thus by determining the gas abundances with the aid of shock models (Raymond 1979; Shull & McKee 1979; DBDB), we can probe the abundances of the ISM into which a SNR is expanding.

The effects of abundances and shock conditions on the optical spectra can be derived from detailed modeling of individual spectra (e.g., Russell & Dopita 1990; Raymond et al. 1988). Alternately, with a sample of SNRs, one may interpolate between sets of shock models assuming that, while individual abundance estimates may not be precise, mean abundances and abundance trends can be accurately derived. Although considerable progress in modeling shocks has been made since 1984, the grid of shock models presented in DBDB remains the most applicable for SNR abundance determination. BK note that the assumption that all observed remnants have shock

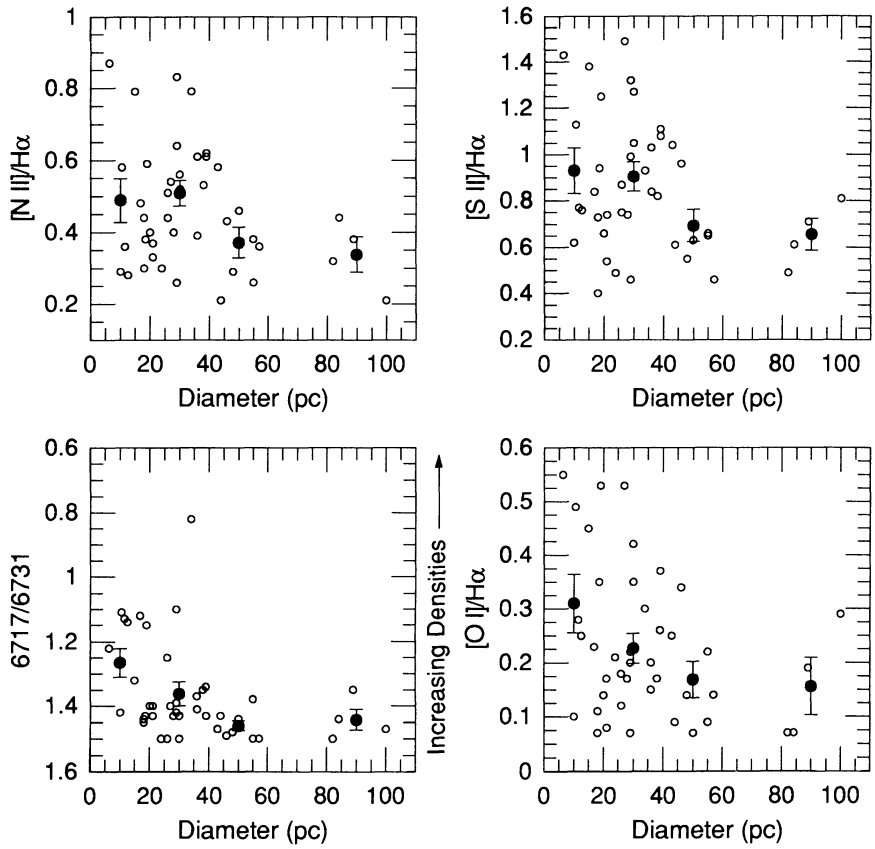

FIG. 7.—Variation of emission-line ratios with SNR diameters. The filled circles are the means of 20 pc wide bins centered at 10, 30, 50, 70, and 90 pc. No increase in the ratios with diameter is evident. There is a marginal decrease in the mean and standard deviation with increasing diameters, but the reality of these trends is questionable due to the small number of remnants at large diameters.

velocities $\gtrsim 100$ km s^{-1} made in these models may adversely affect abundance estimates for low shock velocity remnants. The problem is discussed mostly with respect to the [O III]/Hβ ratio variations caused by low shock velocities, since they relied upon [O III]/Hβ for all abundance determinations from Figures 10 and 11 of DBDB. Figure 5 from DBDB shows that the [O III] line is actually the *most* sensitive to shock velocity variations, falling sharply for shock velocities $\lesssim 100$ km s^{-1}.

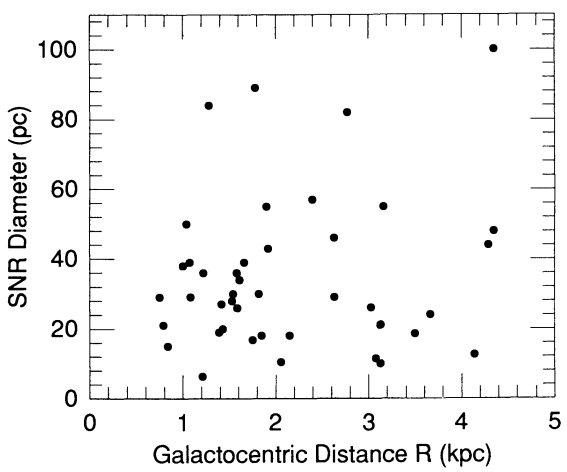

FIG. 8.—The distribution of SNR diameters with distance from the center of M33. No correlations or biases are evident.

The [N II] line intensity falls off the shock velocities less than ~ 80 km s^{-1}, and the [S II] λ6731 line varies by only ~ 0.2 dex down to 50 km s^{-1}. Thus one would expect abundances derived from the [N II] and [S II] λ6731 lines to be less susceptible to variations in shock conditions, at least down to ~ 80 km s^{-1}.

The [N II]/Hα ratio has long been considered a good tracer of relative nitrogen abundances. The [N II] lines are not major coolants, and the [N II] and Hα emission lines are formed at similar temperatures; hence they come from the same post-shock cooling region. These characteristics lead to a relative insensitivity to shock conditions such as shock velocities and preshock densities. Variations in the [N II]/Hα ratio have therefore often been used to demonstrate abundance trends independent of absolute (model-dependent) abundance determinations. In Figure 9, we show the observed variation of [N II]/Hα with increasing distance from the center of M33. A marked decrease in the ratio as one moves out in the disk is apparent, indicative of a significant gradient in the abundance of nitrogen.

The [S II] $\lambda\lambda$6717, 6731 lines are sensitive to collisional deexcitation, hence their density sensitivity, and therefore the [S II]/Hα ratio is more likely to be affected by varying shock conditions. However DBDB argue that use of only the [S II] λ6731 line with respect to Hα removes most of the density sensitivity, leaving abundance effects as the major contributor to observed variations. Indeed, DBDB's Figures 5 and 6 indicate that the 6731/Hα ratio is the least sensitive to shock velocity of all the strong SNR emission lines.

TABLE 4

M33 SNR ABUNDANCES

Name	R (kpc)	N abundance log(N/H)+12	O abundance log(O/H)+12	"Metal" Abundance log A[a]
013004+30226	4.29	7.11	8.05	-4.01
013004+30228	4.35	7.23	7.95	-4.04
013007+30252	4.35	7.12	8.23	-3.88
013008+30241	4.14	7.28	8.31	-3.78
013015+30245	3.66	7.23	7.82	-4.12
013021+30241	3.16	7.37	8.12	-3.87
013021+30270	3.50	7.42	8.40	-3.67
013022+30190	2.77	7.26	7.87	-4.08
013022+30244	3.08	7.40	8.34	-3.72
013040+30269	2.06	7.72	8.77	-3.32
013042+30182	1.61	7.85	8.74	-3.30
013042+30269	1.90	7.19	8.03	-3.99
013047+30211	1.08	7.73	8.61	-3.43
013048+30175	1.54	7.70	8.74	-3.35
013049+30248	1.07	7.70	8.59	-3.46
013049+30270	1.43	7.39	8.12	-3.87
013052+30272	1.28	7.42	8.05	-3.90
013055+30208	0.79	7.34	7.97	-3.99
013059+30177	1.53	7.40	8.19	-3.81
013101+30201	1.00	7.55	8.32	-3.68
013102+30285	1.04	7.44	8.08	-3.88
013105+30185	1.58	7.42	8.31	-3.73
013106+30178	1.75	7.52	8.42	-3.62
013108+30196[b]	1.42	...	...	...
013109+30168	2.15	7.23	7.73	-4.18
013109+30225[b]	0.84	...	...	...
013110+30182	1.85	7.44	8.20	-3.80
013110+30210[b]	1.21	...	...	...
013111+30270[b]	0.75	...	...	...
013113+30157	2.63	7.47	8.40	-3.65
013114+30294	1.22	7.68	8.53	-3.50
013118+30210	1.78	7.38	8.19	-3.82
013121+30271[b]	1.39	...	...	...
013124+30198	2.39	7.30	7.71	-4.17
013125+30244	1.82	7.58	8.49	-3.56
013125+30266	1.66	7.70	8.59	-3.46
013126+30176	3.03	7.44	8.17	-3.81
013128+30260	1.92	7.63	8.48	-3.55
013130+30184	3.13	7.24	8.07	-3.95
013131+30186	3.13	7.32	8.18	-3.85
Average of M33 SNR sample		7.43	8.24	-3.77
std. dev.		0.19	0.28	0.24
Average from M33 HII regions[c]		7.01	8.30	-3.82
std. dev.		0.21	0.20	0.17
Solar abundances[d]		7.94	8.84	-3.18
Galactic SNRs[e]		7.94	8.59	-3.37
std. dev.		0.25	0.28	0.29
Galactic HII regions[f]		7.58	8.75	-3.40
std. dev.		0.30	0.32	...
LMC SNRs[g]		7.45	8.25	-3.76
std. dev.		0.19	0.25	...
LMC HII regions[g]		7.07	8.37	-3.76
std. dev.		0.20	0.22	...

[a] A = generalized "metal" abundance, as defined by DBDB.
[b] Saturated [S II] λ6731, indicative of high abundances.
[c] Based on abundances from Kwitter & Aller 1981.
[d] Cameron 1982.
[e] Based on abundances from FBK.
[f] Based on abundances from Shaver et al. 1983.
[g] Russell & Dopita 1990.

With the grids of shock models from DBDB, we can estimate the absolute nitrogen and oxygen abundances for each of the M33 remnants using the [N II]/Hα and 6731/Hα line ratios, ratios which are well determined from our spectra. DBDB note that competition between the coolant lines means that absolute abundances (or, alternatively, abundances relative to oxygen) cannot be derived from a single line ratio such as [N II]/Hα. Figure 8 from DBDB provides a grid using both [N II]/Hα and 6731/Hα from which we can derive oxygen abundances and N/O ratios. Since we use the [S II] line strength, together with [N II], to determine the nitrogen and oxygen abundances, we cannot derive sulfur abundances with our data set. In fact, in using DBDB's Figure 8, we have implicitly assumed an O/S ratio of 42.8, on which these grids of models were based. DBDB conclude that $O/S = 45 \pm 15$ for extragalactic SNRs, with only a factor of 2 variation over an

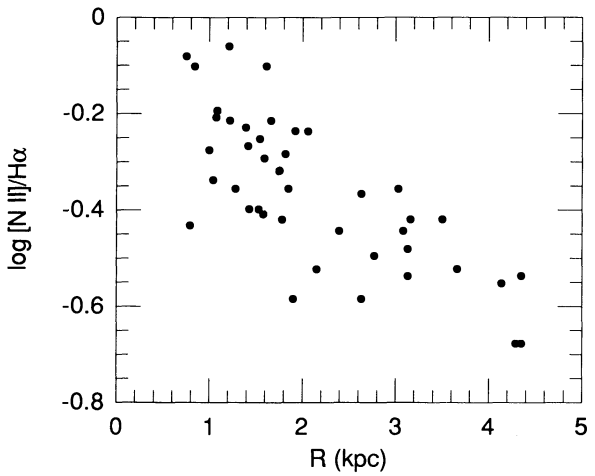

FIG. 9.—The [N II]/Hα gradient in M33 SNRs. Since [N II]/Hα is largely independent of shock conditions, it is an accurate tracer of relative N abundances.

abundance range of ~16. In their sample of 13 M33 remnants, BK found a mean O/S ratio of 55 with a standard deviation of 20, and variations from 22 to 90, in agreement with DBDB's conclusions. Additionally, the correlation shown in Figure 10 between the [O I] line strengths, which is somewhat sensitive to oxygen abundances (DDB), and [S II] line strengths supports the conclusion that the [S II] line does follow the oxygen abundance, although the sensitivity of the [O I]/Hα line ratio to shock conditions has not been fully explored in the literature.

For 6731/Hα ratios $\gtrsim$0.55 the [S II] line saturates and abundances are not uniquely determined by the grid of models presented by DBDB. Five of our 42 SNRs have 6731/Hα ratios $\geq$0.55. No abundance estimates are viable for these five remnants, although their positions on the grid are indicative of high oxygen abundances. Three of these SNRs lie in a region outside the model grid; thus *none* of the DBDB models fit these remnants. It is significant to note that all of these five remnants lie within 1.5 kpc of the galactic center.

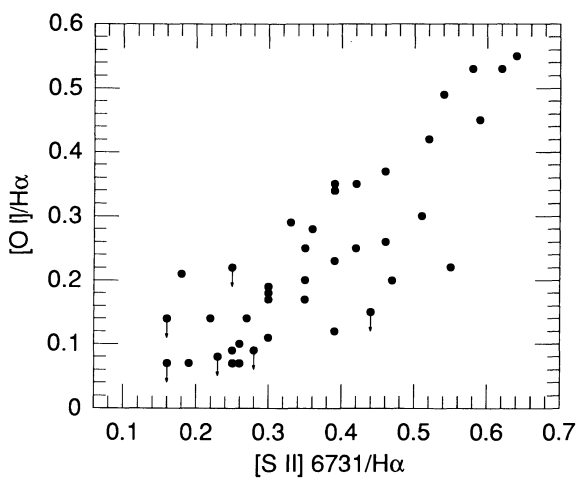

FIG. 10.—The observed correlation of [S II] λ6731 with [O I]. Both trace the O abundance, and the roughly linear relation suggests a roughly constant O/S ratio.

5.3. *Abundances and Abundance Gradients*

The nitrogen and oxygen abundances estimated using DBDB's models for our sample of M33 SNRs are listed in Table 4. We have also calculated the "metal" abundance parameter *A*, as defined in DBDB, again assuming a constant O/S ratio of 42.8. For comparison, the mean values of the abundances from Kwitter & Aller's (1981) study M33 H II regions are given, as well as the mean abundances for Galactic and LMC SNRs and H II regions. It is apparent that the M33 abundances are very similar to those in the LMC and significantly less than those in our Galaxy. It is also interesting to note that the width of all of the distributions are about the same, between roughly 0.2 and 0.3 dex, although this may be due to the limited number of SNRs in all of the samples.

Figure 11 shows the variation in abundances with galactocentric distance for the SNRs (*filled circles*), as well as that for H II regions (*open squares*), as derived from the abundances

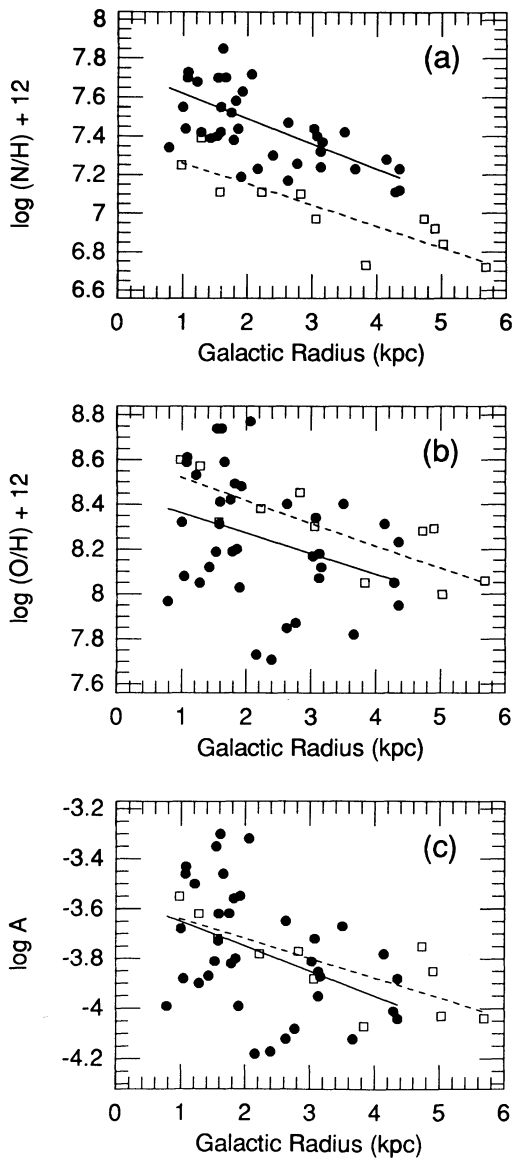

FIG. 11.—Abundance gradients in M33: solid circles are SNRs (this paper), open squares are H II regions (Kwitter & Aller 1981).

TABLE 5

ABUNDANCE GRADIENTS FOR M33 SNRs AND H II REGIONS

	Mean Value 12+log(X/H)	Slope log(X/H)/kpc	Intercept log(X/H) @ R=0	Correlation Coefficient
Nitrogen abundance gradient				
SNRs - this paper	7.47±0.03	-0.14±0.03	7.76±0.06	0.69
SNRs - BK	7.51±0.02	-0.10±0.03	7.77±0.08	0.72
HII regions - KA81	7.01±0.06	-0.11±0.02	7.37±0.08	0.86
Oxygen abundance gradient				
SNRs - this paper	8.24±0.05	-0.09±0.05	8.45±0.12	0.33
SNRs - BK	8.52±0.05	-0.05±0.05	8.64±0.14	0.27
HII regions - KA81	8.30±0.06	-0.10±0.02	8.62±0.09	0.81
HII regions - ZEH89	...	-0.09±0.02	...	...
"Metal" Abundance gradient				
SNRs - this paper	-3.77±0.04	-0.10±0.04	-3.55±0.10	0.41
SNRs - BK	-3.61±0.03	-0.09±0.02	-3.38±0.06	0.77
HII regions - KA81	-3.82±0.05	-0.08±0.02	-3.56±0.08	0.79

REFERENCES.—KA81: Kwitter & Aller 1981; ZEH89; Zaritsky, Elston, & Hill 1989.

given by Kwitter & Aller (1981). The solid and dashed lines are least-squares fits to the SNR and H II region data, respectively. The fitted parameters are summarized in Table 5, as are fits to the previous M33 SNR sample (BK). Note that the uncertainties quoted in Table 5 are the statistical errors derived from the abundance estimates and do not include uncertainties in the derivation of the abundances.

The oxygen abundances show a marginal gradient. Although the best-fit line is inconsistent with no slope, the correlation is extremely weak. The least-squares slope is, however, the same as that determined from the H II region of samples of both Kwitter & Aller (1981) and the empirical analysis of Zaritsky et al. (1989). The evidence for an abundance gradient is strengthened by the five SNRs excluded from this plot, all of which show strong [S II]/Hα ratios evident of large O abundances and are at $R < 1.5$ kpc.

The large scatter in these SNR abundances may be due to variations in shock velocities (and other conditions) despite the supposedly less sensitive line ratios used. The scatter may also be a result of our assumption of a constant O/S ratio, indicating that this ratio is not as limited as DBDB claim. Uncertainties in the O/C ratio may also cause some scatter. Alternately, the scatter may be due to contamination of the SNR ratios by background H II region emission. BK showed that at least one of the 13 remnants they studied required significant correction for background H II region based on high-resolution spectra. Such contamination would drive the ratios down, resulting in smaller oxygen abundance estimates. Indeed, the mean SNR O abundance is slightly (although *not* significantly) lower than that derived from the H II regions.

However, we cannot dismiss the possibility that these large oxygen abundance variations may be real. The observed variation in Galactic abundances, based on both SNRs and H II regions, is similar to that observed in M33 SNRs, and the LMC variations are only slightly smaller. While the scatter in abundances from the 11 M33 H II regions studied by Kwitter & Aller (1981) is smaller than that observed for the SNRs, Zaritsky et al. (1990) state that the abundances in their larger sample of H II regions range over 0.9 dex, similar to our 1.1 dex range (they do not report a standard deviation). Thus it is reasonable to surmise that the standard deviation of 0.28 represents the spread of oxygen abundances in the interstellar gas in M33, although this deduction is impossible to confirm given the uncertainties.

The trend in "metal" abundances is dominated by the scatter introduced by the oxygen abundances, which are doubly weighted since we relied upon a constant O/S ratio to derive them. The relation (Fig. 11*c*) shows a significant slope (mostly due to the nitrogen abundances) but a weak correlation due to the large scatter. As in the case of oxygen, the gradient is consistent with that determined from H II regions (Table 5).

The nitrogen abundances show the most significant gradient (Fig. 11*a*). Although the *gradient* is consistent with that determined from H II regions, the SNR nitrogen abundances are systematically ~0.4 dex larger. This is the same offset that BK noted in their smaller sample of M33 SNRs. As shown in Table 4, Galactic and LMC SNRs and H II regions show similar offsets in nitrogen abundances. BK also found an offset in M31 in their reanalysis of the observations of Blair et al. (1982).

The difference in the nitrogen abundances determined from SNRs and H II regions remains perplexing. As mentioned above, it is extremely unlikely that any ejecta contaminates the SNR emission. Indeed, it is difficult to conceive of any process that selectively enhances the nitrogen abundances. It may be an artifact introduced by the models, but it is unclear which abundances are inaccurate. Evans & Dopita (1985) mention that there is an apparent discrepancy between their modeled and observed [N II] line strengths in H II regions while Russell & Dopita (1990) refer to difficulties in fitting the nitrogen lines in LMC and SMC SNRs. While the H II region abundances in Table 4 are derived from several different models, all of the SNR abundances listed are based on the diagnostic diagrams in DBDB. However, BK claim that calculations based on updated versions of Raymond's (1979) models give nitrogen abundances comparable to those from the DBDB models.

Detailed modeling of spectra with greater wavelength coverage than that presented here may aid in understanding this dilemma.

6. SUMMARY

We have presented optical spectroscopy of all of the SNRs and SNR candidates identified in our imaging survey of the central portion of M33. The [S II]/Hα ratios derived from our Hα and [S II] images agree with the more accurate spectral ratios to within ± 0.1–0.2 for [S II]/Hα $\lesssim 1$, demonstrating that our imaging identification of SNR candidates is accurate. The detection of [O I] emission in all but six of the candidates provides additional evidence that the identified nebulae are shock heated, as opposed to photoionized, nebulae. While there may be some confusion for very low surface brightness nebulae, the existing evidence indicates that all 32 of the candidates are SNRs.

We find no correlation of emission-line ratios with diameter, such as those reported in the Galactic and LMC samples of SNRs by Daltabuit et al. (1976) and D'Odorico & Sabbadin (1976). Assuming that the true (complete) samples of SNRs in the Galaxy and M33 are similar, this result supports the claim of Binette et al. (1982) and FBK that the Galactic trends are due to selection effects. The same selection problems do not apply in the LMC, however, and thus the trends there remain enigmatic, though possibly simply a result of the small sample of SNRs used.

Nitrogen and oxygen abundances for our M33 SNR sample were derived using the grid of models from DBDB. The mean abundances are significantly lower than those in our Galaxy (Shaver et al. 1983; FBK), but similar to those derived for the LMC (Russell & Dopita 1990). There is marginal evidence for an oxygen abundance gradient in the SNRs similar to that derived based on the abundances from H II regions of Kwitter & Aller (1981). The nitrogen abundances show a significant gradient consistent with that derived from H II regions. However, the nitrogen abundances from SNRs are systematically higher by ~ 0.4 dex. This offset has also been noted in studies of SNRs and H II regions in our Galaxy, the LMC, and M31. The source of the discrepancy remains uncertain.

Although the 45 SNRs (including the three confirmed SNRs outside our survey region) in M33 represent the largest extragalactic sample currently available, we have covered only approximately half of the disk in our initial survey of M33. We have obtained additional images covering the whole of the galaxy and are currently working on identifying additional candidates. A recently conducted radio survey of M33 is also yielding promising results, confirming several of the optically selected SNRs and identifying several new candidates (Duric 1988; Gordon 1991). Additionally, X-ray observations with the *ROSAT* satellite hold significant promise.

Spectroscopically, greater wavelength coverage, at least down to [O II] λ3727 if not well into the ultraviolet, would allow more detailed modeling of the shocks. Combined ultraviolet and optical spectra provide much more powerful shock diagnostics than do optical spectra alone. While all but the brightest of the M33 remnants are too faint for *IUE*, many may be within reach of the *Hubble Space Telescope*. Such observations allow shock velocities to be estimated, allowing more confident abundance estimates as well as insight into the evolutionary trends present in the M33 SNR sample.

We would like to thank the staff of the Multiple Mirror Telescope for their help in making these observations successful, and John Raymond for his assistance in interpreting the emission line ratios. This research was partially supported by NSF grant AST-89-05529 to Harvard University (R. P. K.) and NSF grant AST-9114935 to Middlebury College (P. F. W.).

REFERENCES

Bandiera, R. 1987, ApJ, 319, 885
Binette, L., Dopita, M. A., D'Odorico, S., & Benvenuti, P. 1982, A&A, 115, 315
Blair, W. P., & Kirshner, R. P. 1985, ApJ, 289, 582 (BK)
Blair, W. P., Kirshner, R. P., & Chevalier, R. A. 1981, ApJ, 247, 879
———. 1982, ApJ, 254, 50
Blair, W. P., Raymond, J. C., Danziger, J., & Matteucci, F. 1989, ApJ, 338, 812
Cameron, A. G. W. 1982, in Essays in Nuclear Astrophysics, ed. C. A. Barnes, D. D. Clayton, & D. N. Schramm (Cambridge: Cambridge Univ. Press), 23
Chevalier, R. A. 1975, ApJ, 200, 698
Chevalier, R. A., & Kirshner, R. P. 1979, ApJ, 233, 154
Cowan, J. J., & Branch, D. 1985, ApJ, 293, 400
Daltabuit, E., D'Odorico, S., & Sabbadin, F. 1976, A&A, 52, 93
Danziger, I. J., Murdin, P. G., Clark, D. H., & D'Odorico, S. 1979, MNRAS, 186, 55
de Jager, G., & Davies, R. D. 1971, MNRAS, 153, 9
de Vancouleurs, G. 1978, ApJ, 223, 730
de Vancouleurs, G., & Leach, R. 1981, PASP, 93, 190
Deul, E. R., & van der Hulst, J. M. 1987, A&AS, 67, 509
D'Odorico, S. 1978, Mem. Soc. Astr. Ital., 49, 563
D'Odorico, S., Benvenuti, P., & Sabbadin, F. 1978, A&A, 63, 63
D'Odorico, S., Dopita, M. A., & Benvenuti, P. 1980, A&AS, 40, 67
D'Odorico, S., Goss, W. M., & Dopita, M. A. 1982, MNRAS, 198, 1059
D'Odorico, S., & Sabbadin, F. 1976, A&A, 53, 443
———. 1977, A&AS, 28, 439
Dopita, M. A. 1979, ApJS, 40, 455
Dopita, M. A., Binette, L., D'Odorico, S., & Benvenuti, P. 1984, ApJ, 276, 653 (DBDB)
Dopita, M. A., D'Odorico, S., & Benvenuti, P. 1980, ApJ, 236, 628 (DDB)
Dopita, M. A. 1977, ApJS, 33, 437
Duric, N. 1988, in IAU Colloq. 101, Supernova Remnants and the Interstellar Medium, ed. R. S. Roger & T. L. Landecker (Cambridge: Cambridge Univ. Press), 289
Evans, I. N., & Dopita, M. A. 1985, ApJ, 58, 125
Fesen, R. A., Blair, W. P., & Kirshner, R. P. 1985, ApJ, 292, 29 (FBK)
Fusco-Femiano, R., & Preite-Martinez, A. 1984, ApJ, 281, 593
Gordon, S. 1991, private communication
Goss, W. M., Ekers, R. D., Danziger, I. J., & Israel, F. P. 1980, MNRAS, 193, 901
Goss, W. M., & Viallefond, F. 1985, JApAstr, 6, 145
Green, D. A. 1984, MNRAS, 209, 449
———. 1991, PASP, 103, 201
Gull, S. F. 1973, MNRAS, 162, 135
Hawley, S. A. 1978, ApJ, 224, 417
Jacoby, G. 1987, NOAO Newsletter, No. 9, 15
Kent, S. 1987, AJ, 94, 306
Kirshner, R. P., & Winkler, P. F. 1985, ApJ, 299, 981
Kwitter, K. B., & Aller, L. H. 1981, MNRAS, 195, 939
Long, K. S., Blair, W. P., Kirshner, R. P., & Winkler, P. F. 1990, ApJS, 72, 61 (Paper I)
Long, K. S., D'Odorico, S., Charles, P. A., & Dopita, M. A. 1981a, ApJ 246, L61
Markert, T. H., & Rallis, A. D. 1983, ApJ, 275, 571
Mathewson, D. S., & Clarke, J. N. 1972, ApJ, 178, L105
———. 1973, ApJ, 180, 725
Mathewson, D. S., Ford, V. L., Dopita, M. A., Tuohy, I. R., Long, K. S., & Helfand, D. J. 1983, ApJS, 51, 345
Mathewson, D. S., Ford, V. L., Dopita, M. A., Tuohy, I. R., Mills, B. Y., & Turtle, A. J. 1984, ApJS, 55, 189
Mathewson, D. S., Ford, V. L., Tuohy, I. R., Mills, B. Y., Turtle, A. J., & Helfand, D. J. 1985, ApJS, 58, 197
Mathewson, D. S., & Healy, J. R. 1964, in IAU Symp. 20, The Galaxy and the Magellanic Clouds, ed. F. J. Kerr & A. W. Rodgers (Canberra: Australian Academy of Science), 245
McCall, M. L., Rybski, P. M., & Shields, G. A. 1985, ApJS, 57, 1
McKee, C. F. 1974, ApJ, 188, 335
Raymond, J. C. 1979, ApJS, 39, 1
Raymond, J. C., Hester, J. J., Cox, D., Blair, W. P., Fesen, R. A., & Gull, T. R. 1988, ApJ, 324, 869
Reynolds, S. P., & Fix, J. D. 1987, ApJ, 322, 671
Russell, S. C., & Dopita, M. A. 1990, ApJS, 64, 93
Sabbadin, F. 1977, A&A, 54, 915
———. 1978, PASP, 90, 563

Sabbadin, F. 1979, A&A, 80, 212
Sabbadin, F., & Bianchini, A. 1979, PASP, 91, 62
Schmidt, G. D., Weymann, R. J., & Foltz, C. B. 1989, PASP, 101, 713
Searle, L. 1971, ApJ, 168, 327
Shaver, P. A., McGee, R. X., Newton, L. M., Danks, A. C., & Pottasch, S. R. 1983, MNRAS, 204, 53
Shull, J. M., & McKee, C. F. 1979, ApJ, 227, 131
Trinchieri, G., Fabbiano, G., & Peres, G. 1988, ApJ, 325, 531
van den Bergh, S. 1991, PASP, 103, 609
Viallefond, F., Goss, W. M. van der Hulst, J. M., & Crane, P. C. 1986, A&AS, 64, 237
Westerlund, B. E., & Mathewson, D. S. 1966, MNRAS, 131, 371
Zaritsky, D., Elston, R., & Hill, J. M. 1989, AJ, 97, 97
———. 1990, AJ, 99, 1108